PICOSECOND TRIPLET STATE DYNAMICS AND PHOTODISSOCIATION IN 2- AND 9-IODOANTHRACENE*

R.L. PINEAULT, C.G. MORGANTE and W.S. STRUVE

Department of Chemistry and Ames Laboratory, Iowa State University, Ames, IA 50011 (U.S.A.)

Summary

Picosecond-resolved transient absorption spectra of iodoanthracenes excited in the S_1 manifold with about 3000 cm^{-1} excess energy, combined with earlier fluorescence studies and analyses of photoproducts from the 366 nm dissociation of the C–I bond in benzene and cyclohexane solution, give kinetic evidence for the specific intersystem crossing (ISC) and internal conversion (IC) processes which proceed and compete with photodissociation. Since ISC is heavy atom accelerated to the picosecond domain in iodoanthracenes, intramanifold vibrational relaxation as well as triplet–triplet IC can be monitored with approximately 10 ps resolution. The vibrationless T_1 state at about 12 000 cm^{-1} lies below the energy threshold for dissociation so that the quantum efficiency for C–I homolysis is diminished by triplet–triplet IC processes leading to T_1.

354 nm excitation of 9-iodoanthracene in cyclohexane is followed by rapid vibrational thermalization within the S_1 manifold prior to thermally activated ISC to a triplet state T_n of higher energy than S_1. In a subsequent decay scenario consistent with our 432 nm $T_n \leftarrow T_1$ transient absorption rise time and T_1 formation quantum yield, T_n branches into IC (ultimately leading to a long-lived T_1 state) and photodissociation into $R \cdot + I(^2P_{3/2})$ with efficiencies of about 0.2 and 0.8 respectively. The T_1 formation rise time of about 50 ps matches the $S_1 \rightarrow S_0$ fluorescence lifetime within experimental scatter for 9-iodoanthracene in cyclohexane at about 25 °C, implying a non-radiative decay rate of greater than about 10^{11} s^{-1} for T_n in our kinetic model.

1. Introduction

Since 1974, our understanding of photodissociation in polyatomics has been augmented largely by molecular beam photofragment angular distribution studies [1 - 3], by photofragment fluorescence measurements in bulk gases excited in the vacuum UV [4, 5] and by the development of a generalized Franck–Condon theory [6 - 8] for photodissociation which emphasizes the kinematic role of initial state and photofragment normal modes. The last-mentioned approach, which deals with details of the photodissociation step itself, casts the transition amplitude

* Paper presented at the Xth International Conference on Photochemistry, Iraklion, Crete, Greece, September 6 - 12, 1981.

0047-2670/81/0000-0000/$02.50

for dissociation in terms of a reaction coordinate overlap integral between the final photofragment continuum state and the vibrational wavefunction of an effective bound state oscillator whose origin and force constant depend on the normal mode properties of both the initial bound state and the photofragments. In triatomics such as HCN, ICN [6] and CO_2 [7] fragment vibrational state distributions from fluorescence studies are found to be in qualitative agreement with those predicted from the Band–Freed model for collinear photodissociation.

Photodissociation in larger polyatomics such as iodobenzene [1] and $Mn_2(CO)_{10}$ [2], however, is complicated by vastly denser vibrational manifolds built on wider varieties of accessible electronic states, giving rise to internal conversion (IC) and/or intersystem crossing (ISC). Evidence for the competition of such electronic relaxation processes with photodissociation has emerged in molecular beam photofragment studies, which monitor the time scale for the overall dissociation process. From a comparison of the predissociation lifetimes of 1-iodonaphthalene and 1-bromonaphthalene excited primarily in their S_2 manifolds, Dzvonik *et al.* [1] inferred that the decay of S_2 probably branches into $S_2 \rightarrow S_1$ IC and predissociation by ISC into a repulsive $^3(\pi,\sigma^*)$ state. The possible processes after excitation of S_1 haloanthracenes are visualized in Fig. 1, which shows π electron single-excitation CI eigenvalues [9] for low-lying optically active singlets with their corresponding triplets in anthracene-h_{10}. These levels are not drastically perturbed by halogenation [10], but an additional low-lying $^3(\pi,\sigma^*)$ dissociative triplet arises from creation of the weak C–X bond. The overall dissociation energies of haloanthracenes are unknown and are bracketed for iodoanthracenes in Fig. 1 by reported pyrolytic and electron impact dissociation energies for iodobenzene and several alkyl iodides [11].

Creation of S_1 with excess vibrational energy may be followed by (a) vibrational thermalization of S_1 in condensed solvents, (b) ISC to one or several of the nearly isoenergetic triplet states (not all of which are shown in Fig. 1, which is limited to states with spatial symmetries optically connected to A_1) and (c) predissociation of S_1 by the $^3(\pi,\sigma^*)$ continuum state.

When ISC (process (b)) occurs, the emergent triplet state T_n may be predissociated by the $^3(\pi,\sigma^*)$ state or may undergo IC to lower triplets, leading ultimately to vibrationally thermalized T_1 in condensed solvents. T_1 may branch into predissociation as well as slow $T_1 \rightarrow S_0$ ISC if its energy exceeds the dissociation threshold, but this is improbable since the C–I dissociation energy in iodobenzene and the T_1 origin in anthracene are about 20 000 cm^{-1} and 12 000 cm^{-1} respectively. The rates of predissociation by ISC from S_1 and by IC from the various T_n hinge on the pertinent bound state effective oscillators and the projection of the $^3(\pi,\sigma^*)$ surface along the dissociation coordinate and cannot be estimated *a priori*.

In this work the $S_1 \rightarrow T_n$ ISC and $T_n \rightarrow \rightarrow T_1$ IC non-radiative processes in 2- and 9-iodoanthracene were probed after excitation of the S_1 state in cyclohexane with 354 nm single pulses of 8 ps full width at half-maximum (FWHM) near 300 K. Because ISC in aryl iodides is accelerated to the picosecond regime via the internal heavy atom effect, these systems offer a unique opportunity for resolving ultrafast IC and photodissociation steps in addition to ISC. Iodoanthracenes, unlike the lighter aryl iodides studied by Dzvonik *et al.* [1], are readily

dissociated at 354 nm. T_1 formation is monitored by picosecond-resolved $T_n \leftarrow T_1$ triplet–triplet absorption (TTA), whose spectrum at long times (longer than 100 ps) is analogous to the TTA spectra of anthracene [12] and 9-bromoanthracene [13]. A calibration of 9-iodoanthracene TTA optical density changes against those of acridine in *n*-hexane (for which the $S_1 \rightarrow T_1$ ISC quantum yield is approximately known [14]) allows bounds to be placed on the $S_1 \rightarrow T_1$ branching fraction in 9-iodoanthracene. This, combined with photochemical product analyses for 9-iodoanthracene excited at 300 and 366 nm in benzene and cyclohexane by a filtered mercury arc, allows an estimate of the predissociation rate and quantum yield.

2. Experimental details

Single 1060 nm laser pulses (approximately 8 ps FWHM) were generated at a repetition rate of 1/60 Hz using a 1.1 m Nd–glass oscillator (ED-2 Brewster–Brewster rod; dimensions, 1.2 cm (diameter) × 15 cm (pumped length)) mode locked with EK 9860 dye in 1,2-dichloroethane, combined with a KD*P Pockels cell driven by 12 kV pulses (approximately 3 ns FWHM) from a laser-triggered spark gap. The mode locking was monitored with an ITT F4502 biplanar photodiode and Tektronix 7704 oscilloscope. The amplification was provided by ED-2 Brewster–Brewster rods with pumped lengths of 15 and 20 cm, and wavelength conversion to the 530 and 354 nm harmonics was accomplished in 2.54 cm angle-phase-matched KD*P crystals.

Time-resolved TTA spectra of iodoanthracenes were obtained using the apparatus shown in Fig. 2. A check on rotational diffusion artifacts in TTA rise times was made by varying the polarization of the 354 nm pulse with a rotatable

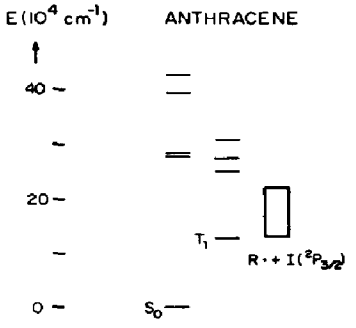

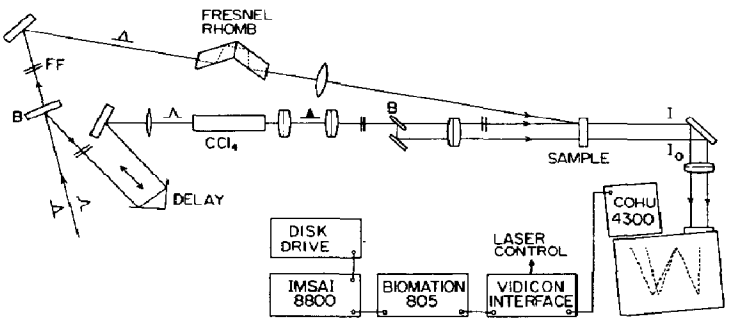

Fig. 1. Low-lying optically active singlet states and corresponding triplet states of anthracene from the electronic structure calculation in ref. 9. Probable dissociation energies of iodoanthracenes into $R\cdot + I(^2P_{3/2})$ are bounded by the rectangle.

Fig. 2. A schematic diagram of the picosecond transient absorption apparatus. The laser, amplifiers and frequency-mixing crystals which generate 1060, 530 and 354 nm single pulses are omitted. The portion of the optical train between the carbon tetrachloride continuum cell and the polychromator is rotated by 90° about the optical axis for clarity: B, beam splitter; FF, UV filters; ⩚, 530 nm; △, 354 nm; ▲, continuum.

Fresnel double-rhomb; the excitation pulse was condensed to a diameter of about 2 mm at the aryl iodide sample in an optical cell of path length 5 mm. Pulse energies (typically 20 μJ) were monitored in a light-shielded HP 4220 diffuser-mounted photodiode and were stored in a Biomation 805 transient recorder. The sample optical density at 354 nm was normally about 1.7.

The 530 nm SHG pulse was passed through a variable optical delay (340 ps range) and focused into a carbon tetrachloride cell of path length 20 cm. (A path length of 20 cm is actually unnecessary [15, 16]: group velocity dispersion in longer cells complicates the interpretation of broad-band transient absorption spectra and limits the effective interaction distances for parametric light generation [17].) The anti-Stokes spectrum of the resulting picosecond broad-band continuum [18, 19] pulse was dynamically compressed between 380 and 480 nm with a 3 mm Corning 1-64 filter and was split by an Inconel-coated neutral beam splitter into a sample probe pulse I and a reference probe pulse I_0. The pulses were achromatically focused at points separated by about 4 mm at the sample, where the I pulse intersected the 354 nm pulse at an angle of about 10°. The probe spectra were then analyzed with a Czerny–Turner Vidicon polychromator (30 cm) with a resolution of 2 nm and a dispersion of 7.9 nm mm^{-1} and were individually imaged about 2 mm apart on an RCA 4532A silicon diode Vidicon grid controlled with a modified Cohu 4300 camera assembly.

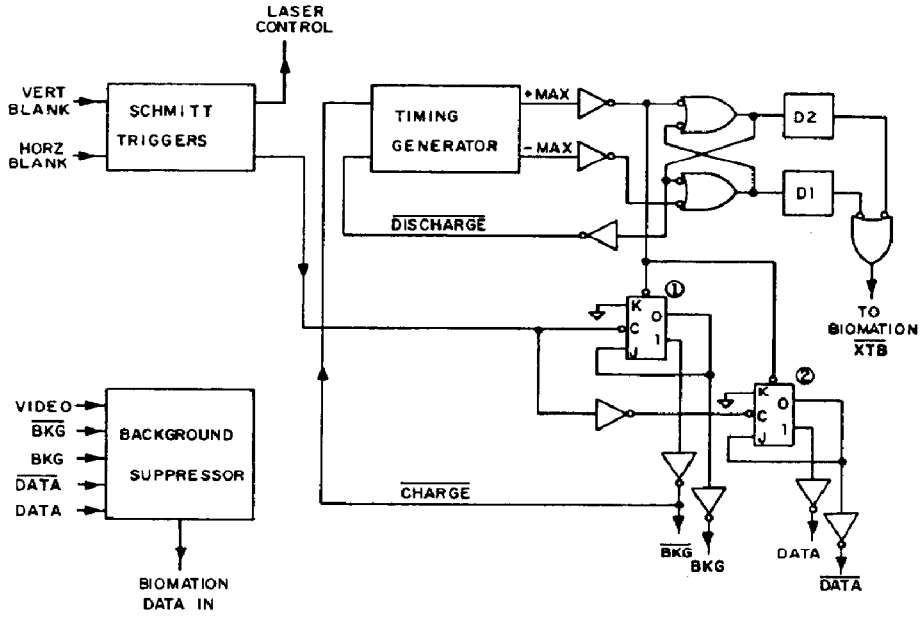

Fig. 3. A block diagram of the Vidicon–Biomation interface for spatially selective strobing of probe and reference continuum spectra into a transient recorder. Horizontal and vertical camera blanking signals are introduced at the upper left-hand side and the video signal enters at the background suppressor input (lower left-hand side). Sampled regions of the Vidicon grid are selected by adjustable delays D1 and D2. The timing generator is described in the text and waveforms are given in Fig. 4.

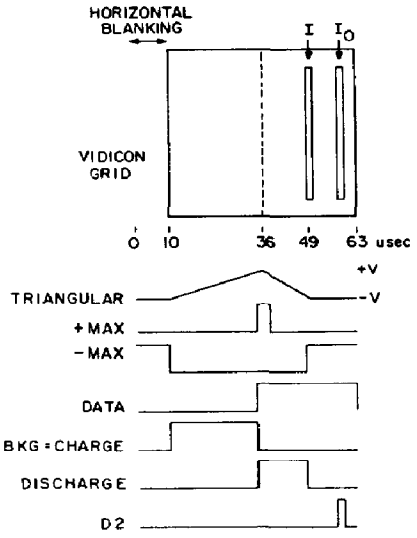

Fig. 4. Vidicon–Biomation interface waveforms during a 15.75 kHz horizontal sweep cycle. The Vidicon grid is divided into background (left-hand side) and signal (right-hand side) halves for dark current suppression; horizontal blanking occupies the first 10 μs of the cycle. I and I_0 spectra are strobed into the Biomation by D1 and D2 pulses. All waveforms, other than triangular, are TTL. The Vidicon was physically mounted sideways to detect horizontally dispersed spectra.

Vidicon dark current suppression and differential storage of the I and I_0 probe spectra (functions commonly supplied with a PARC OMA 2 system) were achieved instead with a custom Vidicon–Biomation 805 interface which is described in the block diagram and waveforms shown in Figs. 3 and 4. Data acquisition was synchronized to the 60 Hz vertical and 15.75 kHz horizontal Vidicon blanking pulses. Adjustable delays between laser flashbank charging and data strobing were obtained by counting vertical blanking pulses, while differential data storage during horizontal sweeps was locked to the (fluctuating) horizontal blanking frequency using the timing generator shown in Fig. 3.

The timing generator input signals $\overline{\text{CHARGE}}$ and $\overline{\text{DISCHARGE}}$ (Fig. 4) alternated the input of an integrating operational amplifier between regulated d.c. voltages $+V$ and $-V$ respectively with different input resistances, creating an asymmetrical triangular waveform peaking at the midpoint and grounding at the three-quarters point of each horizontal sweep. Discriminators converted this into TTL timing generator output signals +MAX and –MAX, on which the detailed timing of data strobing was based. A gated feedback loop through JK-triggered flip-flop 1 in Fig. 3 connected the timing generator inputs $\overline{\text{CHARGE}}$ and $\overline{\text{DISCHARGE}}$ with its outputs ± MAX; clocking flip-flop 1 with the 15.75 kHz blanking frequency locked the strobing cycle (described below) to the horizontal camera sweep.

The unprocessed video signal was gated by the BKG and DATA waveforms (derived from ± MAX, Figs. 3 and 4) to alternating operational amplifiers (configured as lag amplifiers) during the first and second halves of each horizontal

sweep in the background suppressor (Fig. 3). The dark current from the background half-sweep was continuously averaged over about 70 horizontal sweeps, while the total signal from the second half-sweep was updated more than 10^2 times per half-sweep. Cancellation of the dark current was then effected in a difference amplifier with its output directly coupled to the Biomation analog–digital converter.

Selective strobing of I and I_0 probe spectra into the Biomation was furnished by dual monostable delays D1 and D2 respectively. Output from the subsequent NAND gate (Fig. 3) was directed to the Biomation external time base input $\overline{\text{XTB}}$, causing storage of two data words (at delays D1 and D2 adjusted for coincidence with the Vidicon grid locations of the I and I_0 probe spectra) per horizontal sweep. Each laser shot then created a digitized Biomation data array with I and I_0 spectra interlaced in alternating words.

On verification of laser mode locking, each shot of Biomation data was transferred in less than 1 s onto a CP/M-formatted floppy disk by assembler software in an IMSAI 8080 microprocessor. Typically 40 shots were stored per run for various time delays between the pump and probe pulses; additional shots with a spoiled laser cavity were averaged for video baseline subtraction. After data transfer to an Itel AS/5 central computer via a PDP RX11 floppy disk system interface, I and I_0 spectra were computed by pointwise summation over a fixed number of camera frame sweeps. Optical densities $\log(I_0/I)$ were calculated at each of 256 nominal wavelengths about 0.43 nm apart between 380 and 480 nm, and optical density plots were generated using a SIMPLOTTER subroutine on a CalComp plotter.

Representative I and I_0 probe continuum spectra transmitted by 2-iodoanthracene in cyclohexane about 122 ps after excitation are shown with the corresponding TTA spectrum in Figs. 5(a) and 5(b). Blocking of the 354 nm pulse resulted in the optical density baseline in Fig. 5(c); analogous baselines were subtracted from TTA spectra at all time delays.

Beam walkover, satellite pulses, multiphoton absorption, sample saturation and vidicon non-linearity and/or saturation [16] are familiar caveats. The first (arising from variations in pump–probe beam overlap over large optical delay ranges) was insignificant because the normalized 432 nm TTA optical density change of acridine in *n*-hexane [14] was found to be constant within the standard deviation for our apparatus for longer than 150 ps after an induction period of about 90 ps. Satellite pulses from incomplete mode locking were eliminated, since detectable TTA in acridine or iodoanthracene was observed for longer than 10 ps prior to excitation only when double or multiple trains were discernible on the mode-locking monitor. The proportionality of optical density change to pump pulse energy is typified for acridine in *n*-hexane about 122 ps after excitation in Fig. 6. Both acridine and the iodoanthracenes were readily saturated by pumping densities at our disposal, and runs were performed well within the linear range.

Additional experimental considerations in picosecond transient spectroscopy are discussed by Greene *et al.* [16]. We detected an additional potential source of experimental artifacts, arising from angular dispersion in the picosecond continuum generation as a result of non-collinear phase-matched components

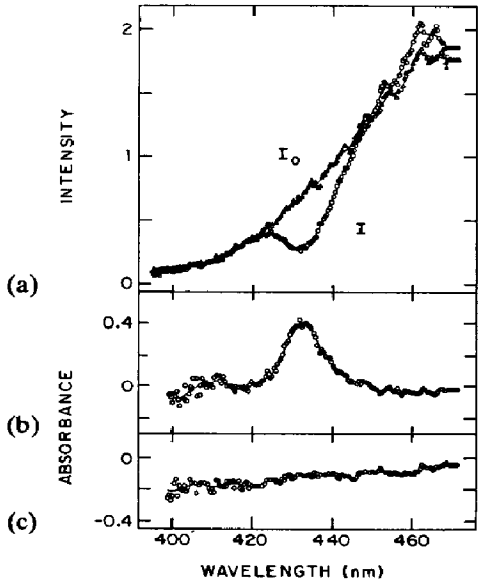

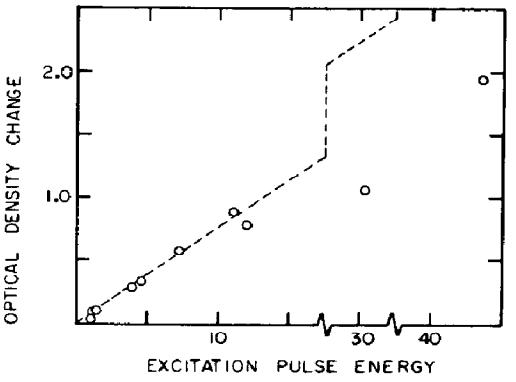

Fig. 5. (a) Single-shot probe and reference continuum pulse spectra transmitted by 2-iodoanthracene in cyclohexane 122 ps after 354 nm excitation; (b) nominal optical density spectrum $\log(I_0/I)$; (c) optical density baseline in the absence of the 354 nm excitation pulse.

Fig. 6. Optical density change derived from plots similar to those in Figs. 5(b) and 5(c) for acridine TTA at 432 nm in *n*-hexane *vs.* pumping energy at 354 nm (an energy of 10 corresponds to about 5 μJ). The excitation pulse diameter at the sample was about 0.1 mm and the probe pulse delay was 122 ps.

(*e.g.* from parametric four-photon emission [15, 17]). As a result, the picosecond continuum pulses were not uniformly focused and overlapped with the excitation pulse in the sample, and the broad-band transient spectrum varied somewhat with both beam alignment and the particular horizontal strips of the I and I_0 spectra selected by the strobe delays D_1 and D_2 (Fig. 4). Single-wavelength transient absorption data are not affected by this phenomenon (described elsewhere).

9-Iodoanthracene was synthesized by catalytic iodination of anthracene in the presence of cupric fluoride by the procedure described by Baird and Surridge [20]. The bulk of the unreacted anthracene was removed by chromatography on Fluorosil and vacuum sublimation, and the 9-iodoanthracene was purified by preparative thin layer chromatography or preparative chromatography. The product was characterized by its mass spectrum and its nuclear magnetic resonance spectrum [21]. 2-Iodoanthracene was prepared by a Grignard synthesis starting with 2-aminoanthracene; its purification and characterization were similar to those for the 9-isomer. The $S_1 \leftarrow S_0$ absorption spectra of the purified iodoanthracenes in cyclohexane contrast with that of zone-refined anthracene (Fig. 7). The maximum of the lowest energy band of 9-iodoanthracene is red shifted relative to that in anthracene owing to the extension of conjugation in S_1 along the short axis by *meso* halogenation [22]; the lowering of the S_1 level by iodination at position 2 is less marked.

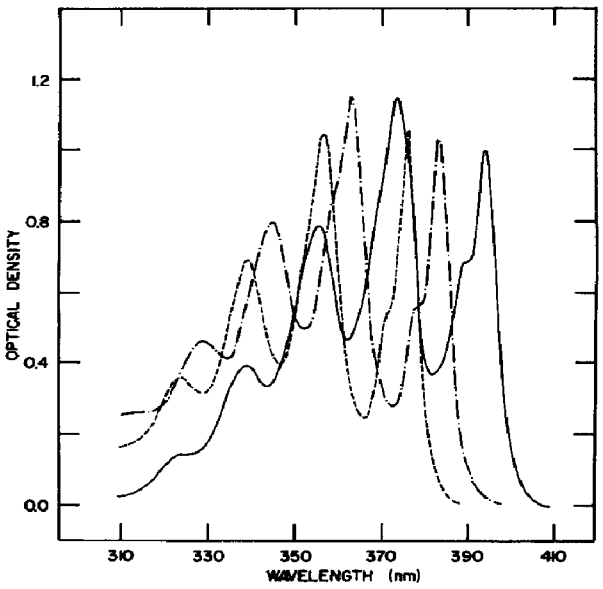

Fig. 7. $S_1 \leftarrow S_0$ absorption spectra of anthracene (– – –), 2-iodoanthracene (– · –) and 9-iodoanthracene (——) in cyclohexane. The absorbances are not mutually normalized.

3. $T_n \leftarrow T_1$ transient absorption

Transient absorption spectra between 380 and 480 nm were obtained for cyclohexane solutions of both iodoanthracene isomers at probe pulse delays ranging from –12.6 to +291.5 ps relative to the 354 nm excitation pulse. Since the refractive index dispersion $dn/d\lambda$ is about -2×10^{-4} nm^{-1} between 430 and 530 nm in carbon tetrachloride [23], the corresponding mean dispersion in continuum delay due to group velocity dispersion alone is –0.13 nm^{-1} in a cell 20 cm long. Delays are therefore specified at 432 nm, the long-time $T_n \leftarrow T_1$ absorption maximum for 2-iodoanthracene in cyclohexane (Fig. 5). The zero delay was determined in separate timing experiments using a carbon disulfide optical shutter cell (0.2 cm) gated by the laser fundamental in place of the aryl iodide sample.

Spectral evolution occurs during the first 50 ps after excitation of the iodoanthracenes, as initially broad triplet–triplet spectra sharpen into well-resolved long-time spectra (Fig. 8) analogous to previously reported TTA spectra of anthracene [12] and 9-bromoanthracene [13] ($\varepsilon_{max} \approx 85\,700$ and $\varepsilon = 66\,500$ respectively at 425 nm). This is similar to the dynamic spectral sharpening observed in TTA of acridine solutions (for long-time acridine TTA spectra see ref. 24; dynamic spectral evolution is described in ref. 16) and gas phase naphthalene [25]. These spectral changes in iodoanthracenes do not uniquely determine a vibrational thermalization time scale in T_1 because the $S_1 \rightarrow T_n$ ISC which precedes the creation of vibrationally hot T_1 by IC is staggered over several tens of picoseconds (the S_1 state lifetime is about 68 ps for 9-iodoanthracene [21]

in cyclohexane at 23 °C). The spectral sharpening cannot be an artifact of group velocity dispersion, which in our apparatus only separates the continuum wavelengths 420 and 440 nm by about 2.5 ps; this is less than the excitation pulse width of about 8 ps.

The time dependence of the 432 nm optical density changes (obtained from subtractions of optical density plots analogous to Figs. 5(b) and 5(c) at each time delay and normalized to the pump pulse energy) is given for both iodoanthracenes in Fig. 9. Since the $^3B_{1g} \leftarrow {}^3B_{2u}$ TTA is polarized normal to the $S_1 \leftarrow S_0$ ($^1B_{2u} \leftarrow {}^1A_{1g}$) excitation transition moment [26], orientational diffusion effects on rise times were eliminated by aligning a probe pulse analyzer 54.7° from the normal to the 354 nm pulse polarization [27]. Data points and standard deviations were computed from at least three laser shots per delay. About 20 additional runs were performed as a check on beam alignment, pumping saturation and orientational relaxation; no observable decay of TTA was found up to 292 ps.

A kinetic model for the photophysical steps after the 354 nm excitation of the iodoanthracenes in cyclohexane (which creates S_1 with about 3000 cm^{-1} of excess vibrational energy in the 9-isomer [21]) may be formulated as follows:

$$S_1\{v\} \xrightarrow{k_T} S_1\{T\} \xrightarrow{K_{ISC}} T_2 \xrightarrow{k_d} \text{photofragments} \qquad (1)$$

$$T_2 \xrightarrow{k_{IC}} T_1$$

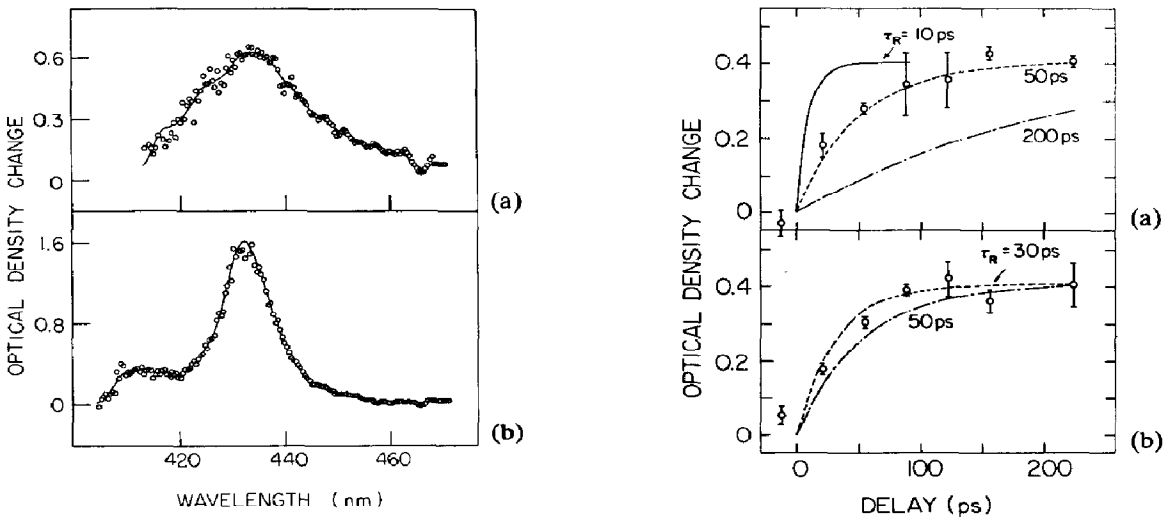

Fig. 8. Transient absorption spectra of 2-iodoanthracene in cyclohexane (a) 19 ps and (b) 122 ps after excitation.

Fig. 9. Time-dependent optical density changes ($\Delta OD(t) = \Delta OD(\infty)\{1 - \exp(-t/\tau_R)\}$) at 432 nm for (a) 9-iodoanthracene in cyclohexane and (b) 2-iodoanthracene in cyclohexane for various rise times τ_R: (a) ——, τ_R = 10 ps; – – –, τ_R = 50 ps; – · –, τ_R = 200 ps; (b) – – –, τ_R = 30 ps; – · – ·, τ_R = 50 ps. The error bars are twice the standard deviation of the normalized optical density changes at each delay.

$S_1\{v\}$ and $S_1\{T\}$ denote Franck–Condon and Boltzmann vibrational populations in the lowest excited singlet state; k_T, k_{ISC}, k_{IC} and k_d are phenomenological rate constants for vibrational thermalization, $S_1 \rightarrow T_2$ ISC (averaged by Boltzmann factors over the S_1 vibrational manifold), $T_2 \rightarrow T_1$ IC and predissociation of T_2 into a repulsive triplet state respectively. In the limit of rapid vibrational thermalization within S_1 ($k_T \gg k_{ISC}$ [21]) the T_1 state population $N_{T_1}(t)$ then obeys

$$N_{T_1}(t) = N_{S_1}(0)\frac{k_{IC}}{k_{IC}+k_d}\left\{1 - \frac{k' \exp(-k_{ISC}t)}{k' - k_{ISC}} + \frac{k_{ISC}\exp(-k't)}{k' - k_{ISC}}\right\} \tag{2}$$

where $k' = k_{IC} + k_d$ denotes the rate constant for first-order decay of T_2. The TTA rise times in Fig. 8, which are well reproduced within scatter by the single exponential function $\Delta OD(t) = \Delta OD(\infty)\{1 - \exp(-t/\tau_R)\}$, are compatible with this kinetic model if $k' = k_{IC} + k_d \gg k_{ISC}$ and if $k_{ISC} = \tau_R^{-1}$. For 9-iodoanthracene the rise time $\tau_R \approx 50$ ps in Fig. 8(a) is consistent with the room temperature fluorescence lifetime [21] of about 68 ps, considering the large standard deviations inherent in the present multishot data and in fluorescence lifetimes evaluated by carbon disulfide optical shutter gating. The rise time for 2-iodoanthracene is nominally shorter (Fig. 8(b)), although the optical density standard deviations are larger than the difference between the optical density changes detected in the two isomers. The S_1 origin of 2-iodoanthracene lies about 700 cm^{-1} above that in the 9-isomer, so that a smaller activation energy for $S_1 \rightarrow T_n$ ISC is anticipated if the triplet levels are comparatively unaffected by halogenation.

The T_1 formation yield in 9-iodoanthracene was standardized to that of acridine in *n*-hexane (which exhibits a 432 nm TTA spectrum [14, 25] akin to that in anthracenes) using samples of equal optical density at 354 nm. The ratio of $S_1 \rightarrow T_1$ ISC quantum efficiencies is related to that of the corresponding long-time 432 nm optical density changes ΔOD by

$$\frac{\varphi_{ISC}{}^{9\text{-IA}}}{\varphi_{ISC}{}^{ACR}} = \frac{\varepsilon_{TT}{}^{ACR} I_p{}^{ACR} \Delta OD^{9\text{-IA}}}{\varepsilon_{TT}{}^{9\text{-IA}} I_p{}^{9\text{-IA}} \Delta OD^{ACR}} \tag{3}$$

where I_p denotes pumping energy and ε_{TT} is the TTA coefficient at 432 nm. The reported value for $\varphi_{ISC}{}^{ACR}$ is 0.4 [14]; approximating $\varepsilon_{TT}{}^{9\text{-IA}}$ by the TTA coefficient for 9-bromoanthracene in cyclohexane then yields an estimated $\varphi_{ISC}{}^{9\text{-IA}}$ of about 0.2 for the $S_1 \rightarrow T_1$ ISC quantum efficiency in 9-iodoanthracene. This implies that $k_{IC}/(k_d + k_{IC}) \approx 0.2$ in kinetic scheme (1) or that $k_d/k_{IC} \approx 4$. The foregoing analysis rests on the assumptions for the TTA coefficient $\varepsilon_{TT}{}^{9\text{-IA}}$ and for $\varphi_{ISC}{}^{ACR}$ as well as on the validity of our kinetic model (which is discussed in Section 4). The spectral FWHM of the 432 nm 2-iodoanthracene TTA spectrum in Fig. 5(b) exceeds that of the 425 nm 9-bromoanthracene peak in cyclohexane [13] by a factor of 1.2 at most. If $\varepsilon_{TT}{}^{9\text{-IA}}$ were (conservatively) half the value of the 9-bromoanthracene TTA coefficient [13] (66500 ± 3250) and if $\varphi_{ISC}{}^{ACR}$ were unity instead of 0.4, we would obtain $k_{IC}/(k_d + k_{IC}) \approx 0.8$, implying that T_1 is still formed with less than unit quantum efficiency.

The rise time data in Fig. 8 furnish only a lower limit for $k_d + k_{IC}$. Since $(k_d + k_{IC})^{-1} \gtrsim 10$ ps would have created a noticeable inflection point characteristic of biexponential growth (eqn. (2)) in Fig. 8, $k_d + k_{IC}$ has a lower bound of about 10^{11} s^{-1}.

Photoproducts from irradiation of benzene and cyclohexane solutions of 9-iodoanthracene by a 200 W high pressure mercury lamp in an optical bench photoreactor were analyzed by high pressure liquid chromatography. The major photolysis products from 9-iodoanthracene exposed to Pyrex-filtered light ($\lambda > 300$ nm) in benzene under argon were 9-phenylanthracene and iodine, with anthracene in smaller yields. The excitation of 9-iodoanthracene in cyclohexane under argon for 1 h at either 313 or 366 nm (10 nm excitation bandpass) yielded about 10% conversion to anthracene, corresponding to a dehalogenation quantum yield of less than 0.1. This is a lower bound to the quantum efficiency for the primary photodissociation because of the extensive geminate recombination of photoproduct radicals (dynamic evidence for the geminate recombination of iodine atoms in iodine solution photodissociation is given in ref. 28).

4. Discussion

Each of the photophysical steps in the proposed kinetic scheme (1) has been extensively explored in other aryl halides. The fluorescence quantum yield [29, 30] and lifetime [21] measurements on 9-haloanthracenes in various solvents have demonstrated that the S_1 state non-radiative decay is markedly temperature dependent. Since the vibrationless T_1 state lies about 12000 cm^{-1} below S_1, the S_1 decay is dominated by $S_1 \rightarrow T_n$ ISC to some higher triplet which lies above S_1 in 9-substituted anthracenes. The presence of such a level has been confirmed by Gillispie and Lim [10], who combined $T_n \rightarrow T_1$ triplet–triplet fluorescence (TTF) spectra (peaking at 800 - 900 nm [10] in substituted anthracenes) with $T_1 \rightarrow S_0$ phosphorescence spectra to show that T_n lies about 330 cm^{-1} and 780 cm^{-1} above S_1 in 9-bromoanthracene and 9,10-dibromoanthracene respectively. The picosecond fluorescence lifetime measurements [21] on 9-iodoanthracene in cyclohexane at 23 and 65 °C provide explicit evidence that vibrational thermalization in S_1 proceeds rapidly compared with ISC from S_1.

Anomalies in TTF quantum yields [31] have cast doubt on the *a priori* plausible assignment of T_n as $T_2(^3B_{1g})$. The TTF quantum yield, assuming that such a T_2 level decays primarily by IC to T_1, would be given by $\varphi_{ISC} k_{T_2 \rightarrow T_1}^{rad} / k_{T_2 \rightarrow T_1}^{IC}$, in terms of the $S_1 \rightarrow T_2$ ISC yield and the rate constants for radiative and non-radiative T_2 state decay. Reasonable estimates are available [31] for φ_{ISC} and $k_{T_2 \rightarrow T_1}^{rad}$; a value of about $(200\ ps)^{-1}$ for the non-radiative IC rates has been inferred indirectly from photosensitization experiments in 9-substituted anthracenes [32]. The combined data project a TTF quantum yield of about 10^{-5}, which exceeds experimental TTF quantum yields by factors of up to 10^3. Hence, the IC rate constant estimated from photosensitization studies may be too small.

Additional evidence that T_1 in non-photoactive anthracenes is populated at a rate appreciably faster than $(200\ ps)^{-1}$ is furnished by recent picosecond

TTA experiments [33] which have shown that rise times of T_1 formation in several nitroanthracenes range from 70 to 90 ps. Since the fluorescence lifetimes of the nitroanthracenes are not known, these rise times provide a minimum value of about 1.4×10^{10} s^{-1} for IC leading to T_1. An interpretation of our TTA rise times for the iodoanthracenes in terms of kinetic model (1) would conservatively require that $k_d + k_{IC} \approx 5\,k_{IC} \geqslant 10 k_{ISC}$, *i.e.* $k_{IC} \geqslant 4 \times 10^{10}$ s^{-1} (or (25 ps)$^{-1}$). Leeway in the parameters employed in calculating the IC and dissociation branching ratios (*e.g.* smaller $\varepsilon_{TT}^{9\text{-IA}}$ or larger φ_{ISC}^{ACR} than used in Section 3) may relax this lower bound somewhat, but it is unlikely that k_{IC} in the iodoanthracenes is as small as (200 ps)$^{-1}$.

In this context, an energy gap law correlation of IC rates compiled by Gillispie and Lim [34] for several $S_1 \rightarrow S_0$ and $T_2 \rightarrow T_1$ processes in aromatic hydrocarbons is of interest. The non-radiative rate may be written using the golden rule expression [35]

$$k_{s\rightarrow l} = \frac{2\pi}{\hbar} \beta_{sl}^2 \sum_n |\langle 0|n\rangle|^2 \delta(\Delta E_{sl} - n\hbar\omega) \tag{4}$$

for IC between a vibrationless electronic state s and the isoenergetic vibronic levels in electronic state l with n quanta in a promoting vibrational mode. Here, β_{sl} is the electronic matrix element of the non-adiabatic coupling, $|\langle 0|n\rangle|^2$ is the Franck–Condon factor between initial and final (displaced) vibrational states and ΔE_{sl} is the electronic energy gap between states s and l. When $n \equiv \Delta E_{sl}/\hbar\omega$ is large, the IC rate reduces to

$$k_{sl} \approx \left(\frac{2\pi\hbar\omega}{\Delta E_{sl}}\right)^{1/2} \frac{\beta_{sl}^2}{\hbar\omega} \exp(-\Delta) \exp\{-n(\ln n/\Delta - 1)\} \tag{5}$$

where $\Delta = \mu\omega(Q_s^\circ - Q_l^\circ)^2/2\hbar$ is a dimensionless parameter which incorporates the reduced mass and the shift equilibrium position for the IC-promoting mode. If the electronic matrix elements β_{sl}, the equilibrium position shifts and the quanta $\hbar\omega$ of the promoting modes vary little between different IC processes in aromatic hydrocarbons [36], the IC rate correlates uniquely with the normal mode structure and the electronic energy gap ΔE_{sl}. Gillispie and Lim have shown that such a correlation is remarkably well borne out for experimental rates of $S_1 \rightarrow S_0$ processes in pentacene, coronene, naphthalene, anthracene and tetracene as well as for the $T_2 \rightarrow T_1$ process in naphthalene: energy gap law projections and experimental IC rates differ by a factor of about 2.5 at most. In this scheme the predicted $T_2 \rightarrow T_1$ IC rate [34] in anthracene ($\Delta E_{sl} \approx 12\,000$ cm^{-1}) is 5×10^9 s^{-1} = (200 ps)$^{-1}$. The cumulative evidence from TTF quantum yields, TTA rise times in nitroanthracenes and the present data thus indicate a breakdown in the energy gap law correlation when applied to $T_2 \rightarrow T_1$ IC in anthracenes.

A possible origin for this discrepancy is the presence of at least one additional triplet state between S_1 and the triplet state populated by ISC from S_1. IC would then proceed rapidly (in the usual sense of the energy gap law) between the nearly degenerate triplets and would be followed by slower IC to T_1 in non-reactive anthracenes. The anomalously low TTF quantum yields may then be explained if the intermediate triplet is not optically connected to T_1 [31]. Ac-

celerated $T_2 \rightarrow = T_1$ IC (relative to the energy gap law prediction) may arise from the proximity effect [37] via vibronic coupling between the closely spaced triplets. If the T_2 and T_3 levels are of $^3B_{3u}$ and $^3B_{1g}$ symmetry as has been suggested [31], they may be coupled by low frequency in-plane b_{2u} skeleton modes. It is not unlikely that near degeneracy occurs between two triplets lying near S_1, considering the local density of electronic triplet states predicted in Fig. 1.

Ultrafast gas phase predissociation of other aryl iodides has been demonstrated by Dzvonik *et al.* [1] in photofragment angular distribution studies of halogen atoms from Hg–Xe arc photolysis of iodobenzene, α-iodonaphthalene and 4-iodobiphenyl. Predissociation lifetimes for these species (excited primarily in their $^1B_{2u}$ and $^1(n,\sigma^*)$, S_2, and ^1L_a states respectively) were inferred from anisotropies in the iodine atom angular distribution and known rotational periods of the aryl iodides and were all found to be less than 1 ps. What, then, accounts for the contrast between the subpicosecond predissociation time scale of these volatile aryl iodides and the primary S_1 state decay in iodoanthracenes, which requires tens of picoseconds? In the Band–Freed formulation [6 - 8] of the rate for predissociation of a vibrationless bound state into a repulsive state for vibrationless fragments, a critical factor in the transition amplitude is an overlap integral along the reaction coordinate Q between the continuum state $S_E(Q)$ and an effective harmonic oscillator wavefunction whose force constant and equilibrium position Q_0 depend on the parent and fragment normal modes:

$$I = \int_{-\infty}^{\infty} dQ\, S_E(Q) \exp\{-y(Q - Q_0)^2\} \tag{6}$$

By approximating $S_E(Q)$ with the Airy wavefunction for a linear repulsive potential with slope F and classical turning point $Q = Q_t$, we obtain [6] an analytical expression for the Franck–Condon factor

$$I \propto \exp\{-\beta^{2/3}(Q_0 - Q_t)\}\ \mathrm{Ai}\left\{\left(\frac{\beta}{4y}\right)^2 - \beta^{1/2}(Q_0 - Q_t)\right\} \tag{7}$$

which decreases rapidly with increasing separation between the effective oscillator position and the repulsive state turning point. (The quantity $\beta = (2\mu F)^{2/3}$ depends on the reduced mass of the photofragments and on the slope of the repulsive potential.)

Possible potential energy curves relevant to predissociation of the volatile iodides (excited between about 33 000 and 42 000 cm^{-1}) and the iodoanthracenes (vibrationally relaxed S_0 state energies of about 25 000 cm^{-1}) are given in Figs. 10(a) and 10(b) respectively. If the C–I bond dissociation energies and projections of $^3(\pi,\sigma^*)$ potential energy surfaces along the reaction coordinate are similar, the bound–continuum overlap integral may increase rapidly with excited singlet energy, depending on the dissociation potential slope F. If predissociation of an initially pumped singlet state is slow (as in Fig. 10(b)), the singlet may decay by ISC into a bound triplet which is subsequently predissociated in a rapid spin-allowed process. The representation in Fig. 10 is necessarily conjectural: there is no reliable basis at present for treating the aryl iodide dissociation energy or dissociative potential as local bond properties, and the variation in singlet state effective oscillator position (tacitly treated as constant in Fig. 10) with the nature

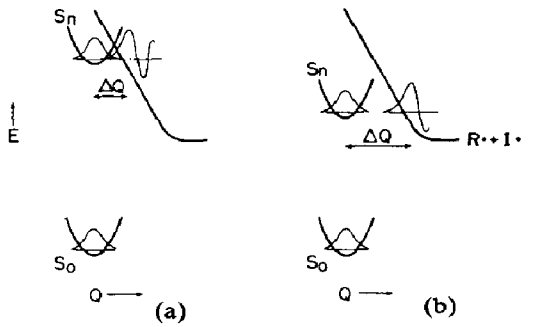

Fig. 10. Bound and continuum states in the reaction coordinate Q for predissociation of aryl iodide singlet states with different energies. The effective oscillator equilibrium position and the repulsive state classical turning point are separated by ΔQ.

of the aryl substrate is difficult to assess. The present role of the solvent bath in S_1 state thermalization also complicates comparisons between our iodoanthracene data and the gas phase photofragment studies, although it is clear that the vibrationless S_1 state in iodoanthracenes is predissociated much more slowly than the singlets excited between 230 and 300 nm in iodobenzene, 4-iodobiphenyl and 1-iodonaphthalene.

Acknowledgments

This work was supported by the U.S. Department of Energy, Division of Chemical Sciences, Contract W-7405-Eng-82, and by the National Science Foundation under Contract CHE-76-80366. We are indebted to Dr. Richard Johnson and Thomas Stierman for the iodoanthracene syntheses and photochemical product analysis. The Vidicon–Biomation interface was ably designed by Harold Skank, and Dr. Mary Gress provided valuable assistance in data analysis.

The Ames Laboratory is a U.S. Department of Energy Facility.

References

1 M. Dzvonik, S. Yang and R. Bersohn, *J. Chem. Phys., 61* (1974) 4408.
2 A. Freedman and R. Bersohn, *J. Am. Chem. Soc., 100* (1978) 4116.
3 A. Freedman, S.C. Yang, M. Kawasaki and R. Bersohn, *J. Chem. Phys., 72* (1980) 1028.
S.C. Yang, A. Freedman, M. Kawasaki and R. Bersohn, *J. Chem. Phys., 72* (1980) 4058.
4 A. Mele and H. Okabe, *J. Chem. Phys., 51* (1969) 4798.
5 L.C. Lee and D.L. Judge, *Can. J. Phys., 51* (1973) 378.
6 Y.B. Band and K.F. Freed, *J. Chem. Phys., 63* (1975) 3382.
7 Y.B. Band and K.F. Freed, *J. Chem. Phys., 64* (1976) 4329.
8 K.F. Freed and Y.B. Band, in E.C. Lim (ed.), *Excited States,* Vol. 3, Academic Press, New York, 1978, pp. 109 - 201.
9 R.L. Hummel and K. Ruedenberg, *USAEC Res. Dev. Rep. IS-450* (Category UC-4, TID-4500), 1964 (Office of Technical Services, Washington, DC).

10 G.D. Gillispie and E.C. Lim, *J. Chem. Phys., 65* (1976) 2022.
11 T.L. Cottrell, *The Strengths of Chemical Bonds,* Academic Press, New York, 2nd edn., 1958.
12 R. Bensasson and E.J. Land, *Trans. Faraday Soc., 67* (1971) 1904.
13 M.B. Ledger and G.A. Salmon, *J. Chem. Soc., Faraday Trans. II, 72* (1976) 883.
14 L.J. Noe, E.O. Degenkolb and P.M. Rentzepis, *J. Chem. Phys., 68* (1978) 4435.
15 R.W. Anderson, D.E. Damschen, G.W. Scott and L.D. Talley, *J. Chem. Phys., 74* (1980) 1134.
16 B.I. Greene, R.M. Hochstrasser and R.B. Weisman, *J. Chem. Phys., 70* (1979) 1247.
17 A. Penzkofer and W. Kaiser, *Opt. Quantum Electron., 9* (1977) 315.
18 R.R. Alfano and S.L. Shapiro, *Chem. Phys. Lett., 8* (1971) 631.
19 G.E. Busch, R.P. Jones and P.M. Rentzepis, *Chem. Phys. Lett., 27* (1974) 31.
20 W.C. Baird, Jr., and J.H. Surridge, *J. Org. Chem., 35* (1970) 3436.
21 C.G. Morgante and W.S. Struve, *Chem. Phys. Lett., 68* (1979) 272.
22 E.C. Lim, J.D. Laposa and J.M.H. Yu, *J. Mol. Spectrosc., 19* (1966) 412.
23 A.L. Dixon and C.J. West, *International Critical Tables,* Vol. VII, 1930, p. 34.
24 E.J. Land, *Proc. R. Soc. London, Ser. A, 305* (1968) 457.
V. Sundstrom, P.M. Rentzepis and E.C. Lim, *J. Chem. Phys., 66* (1977) 4287.
25 H. Schroder, H.J. Neusser and E.W. Schlag, *Chem. Phys. Lett., 54* (1978) 4.
26 R. Pariser, *J. Chem. Phys., 24* (1956) 250.
E.F. McCoy and I.G. Ross, *Aust. J. Chem., 15* (1962) 573.
27 T. Tao, *Biopolymers, 8* (1969) 609.
T.J. Chuang and K.B. Eisenthal, *J. Chem. Phys., 57* (1972) 5094.
28 T.J. Chuang, G.W. Hoffman and K.B. Eisenthal, *Chem. Phys. Lett., 25* (1974) 201.
29 E.J. Bowen and J. Sahu, *J. Phys. Chem., 63* (1959) 4.
30 W.R. Ware and B.A. Baldwin, *J. Chem. Phys., 43* (1965) 1194.
31 G.D. Gillispie and E.C. Lim, *Chem. Phys. Lett., 63* (1979) 355.
32 R.O. Campbell and R.S.H. Liu, *J. Am. Chem. Soc., 95* (1973) 6560.
33 K. Hamanoue, S. Hirayama, T. Nakayama and H. Teranishi, *J. Phys. Chem., 84* (1980) 2074.
34 G.D. Gillispie and E.C. Lim, *Chem. Phys. Lett., 63* (1979) 193.
35 G.W. Robinson, in E.C. Lim (ed.), *Excited States,* Vol. 1, Academic Press, New York, 1974, pp. 4 - 5.
36 P. Avouris, W.M. Gelbart and M.A. El-Sayed, *Chem. Rev., 77* (1977) 793.
37 R.M. Hochstrasser and C.A. Marzzacco, in E.C. Lim (ed.), *Molecular Luminescence,* Benjamin, New York, 1969, p. 631.
N. Kanamaru and E.C. Lim, *J. Chem. Phys., 62* (1975) 3252.